Comparison of magnetic resonance feature tracking for systolic and diastolic strain and strain rate calculation with spatial modulation of magnetization imaging analysis

Moody, William E.; Taylor, Robin J.; Edwards, Nicola C.; Chue, Colin D.; Umar, Fraz; Taylor, Tiffany J.; Ferro, Charles J.; Young, Alistair A.; Townend, Jonathan N.; Leyva, F.; Steeds, Richard P.

DOI:
10.1002/jmri.24623

Original Research

Comparison of Magnetic Resonance Feature Tracking for Systolic and Diastolic Strain and Strain Rate Calculation With Spatial Modulation of Magnetization Imaging Analysis

William E. Moody, MRCP,[1,2]* Robin J. Taylor, MRCP,[1,2] Nicola C. Edwards, PhD,[1,2] Colin D. Chue, PhD,[1,2] Fraz Umar, MRCP,[1,2] Tiffany J. Taylor, MBChB,[2] Charles J. Ferro, MD,[2,3] Alistair A. Young, PhD,[4] Jonathan N. Townend, MD,[1,2] F. Leyva, MD,[1,2] and Richard P. Steeds, MD[1,2]

Purpose: To compare cardiovascular magnetic resonance-feature tracking (CMR-FT) with spatial modulation of magnetization (SPAMM) tagged imaging for the calculation of short and long axis Lagrangian strain measures in systole and diastole.

Materials and Methods: Healthy controls ($n = 35$) and patients with dilated cardiomyopathy ($n = 10$) were identified prospectively and underwent steady-state free precession (SSFP) cine imaging and SPAMM imaging using a gradient-echo sequence. A timed offline analysis of images acquired at identical horizontal long and short axis slice positions was performed using CMR-FT and dynamic tissue-tagging (CIMTag2D). Agreement between strain and strain rate (SR) values calculated using these two different methods was assessed using the Bland–Altman technique.

Results: Across all participants, there was good agreement between CMR-FT and CIMTag for calculation of peak systolic global circumferential strain (−22.7 ± 6.2% vs. −22.5 ± 6.9%, bias 0.2 ± 4.0%) and SR (−1.35 ± 0.42 1/s vs. −1.22 ± 0.42 1/s, bias 0.13 ± 0.33 1/s) and early diastolic global circumferential SR (1.21 ± 0.44 1/s vs. 1.07 ± 0.30 1/s, bias −0.14 ± 0.34 1/s) at the subendocardium. There was satisfactory agreement for derivation of peak systolic global longitudinal strain (−18.1 ± 5.0% vs. −16.7 ± 4.8%, bias 1.3 ± 3.8%) and SR (−1.04 ± 0.29 1/s vs. −0.95 ± 0.32 1/s, bias 0.09 ± 0.26 1/s). The weakest agreement was for early diastolic global longitudinal SR (1.10 ± 0.40 1/s vs. 0.67 ± 0.32 1/s, bias −0.42 ± 0.40 1/s), although the correlation remained significant ($r = 0.42$, $P < 0.01$). CMR-FT generated these data over four times quicker than CIMTag.

Conclusion: There is sufficient agreement between systolic and diastolic strain measures calculated using CMR-FT and myocardial tagging for CMR-FT to be considered as a potentially feasible and rapid alternative.

Key Words: cine magnetic resonance imaging; left ventricular function; tagging; feature tracking
J. Magn. Reson. Imaging 2014;00:000–000.

MYOCARDIAL STRAIN is a sensitive measure of regional and global left ventricular (LV) contractile function (1). Recognizing abnormal strain allows the early detection of subtle LV dysfunction which precedes decreases in ejection fraction in conditions such as dilated cardiomyopathy (DCM) (2,3). Early identification of myocardial dysfunction is important for clinical risk stratification, prompt initiation of treatment, and guides therapeutic decision-making (4). We recently used dynamic tissue-tagging cardiac magnetic resonance (CMR) imaging to identify improvements in longitudinal strain parameters following treatment with spironolactone in patients with early-stage chronic kidney disease (5).

Myocardial tagging by cardiovascular magnetic resonance imaging (MRI) has been widely accepted as

[1]Department of Cardiology, Nuffield House, Queen Elizabeth Hospital Birmingham, Edgbaston, Birmingham, UK.
[2]Centre for Cardiovascular Sciences, School of Clinical and Experimental Medicine, University of Birmingham, Edgbaston, Birmingham, UK.
[3]Department of Nephrology, Queen Elizabeth Hospital Birmingham, Edgbaston, Birmingham, UK.
[4]Centre for Advanced MRI, University of Auckland, Auckland, New Zealand.

Additional Supporting Information may be found in the online version of this article at the publishers website.

The first two authors contributed equally to this work.

Contract grant sponsor: British Heart Foundation Clinical Research Training Fellowship; Contract grant number: FS 11/17/28700 (to W.E.M.); Contract grant sponsor: Birmingham NIHR/Wellcome Clinical Research Facility at the Queen Elizabeth Hospital; Contract grant sponsor: UKCLRN.

*Address reprint requests to: W.E.M., Birmingham Cardio-Renal Group, Clinical Cardiovascular Science, School of Clinical and Experimental Medicine, University of Birmingham, Birmingham, B15 2TT, UK. E-mail: william.moody@nhs.net

Received October 10, 2013; Accepted March 4, 2014.
DOI 10.1002/jmri.24623
View this article online at wileyonlinelibrary.com.

the reference standard noninvasive imaging technique for quantifying strain after validation against sonomicrometry in humans (6) and nonhomogenous strain phantoms (7). Most MR tagging techniques create a visible pattern of magnetization saturation in a grid or with parallel lines on the magnitude reconstructed images which are then analyzed, eg, spatial modulation of magnetization (SPAMM), or by extracting information about myocardial tags in *k*-space, eg, harmonic phase (HARP) (8). All tagging pulse sequences have at least one disadvantage which may include tag fading, low signal-to-noise ratio, long acquisition times requiring prolonged breath-holds, limited availability of validated postprocessing software, and protracted retrospective analysis. Moreover, each tagging technique requires the acquisition of additional sequences to those which are routinely performed, a factor limiting clinical applicability.

Cardiac magnetic resonance feature-tracking (CMR-FT) analysis offers a fast and practical method to calculate strain from routinely acquired steady-state free precession (SSFP) cine images without the need to perform additional tagged sequences (9). In a large study of boys with Duchenne muscular dystrophy, CMR-FT was proposed as an accurate method for measuring strain in a comparison with HARP, although quantification was limited to average circumferential systolic strain in the mid-LV short axis slice (10). Despite recent reports addressing interstudy (11), and inter- and intraobserver variability for CMR-FT (12,13), there has been no attempt to validate this technique for diastolic strain rate (SR) calculation against a reference standard myocardial tagging analysis (14). Furthermore, according to one previous study the CMR-FT framework cannot yet be reliably extended to assess long axis function (15). Therefore, the aim of the current study was to compare CMR-FT with SPAMM tissue tagging for the computation of longitudinal and circumferential systolic *and* diastolic strain measures in a group of healthy adult controls and patients with DCM.

MATERIALS AND METHODS

This study was approved by the West Midlands Research Ethics Committee and carried out in accordance with the principles of the Declaration of Helsinki. All patients provided informed written consent.

Study Population

Control Subjects

Normal healthy adults were identified from an ongoing prospective, observational research study examining the effects of living kidney donation on cardiovascular structure and function (REC: 10/H1207/70). The current UK exclusion criteria for living kidney donation include: diabetes mellitus, any history of cardiovascular or pulmonary disease, evidence of hypertensive end organ damage, LV systolic dysfunction, and atrial fibrillation. Prior to nephrectomy, all potential kidney donors who underwent normal baseline cardiac MR studies from March 2011 to June 2012 were included as healthy controls. Control subjects also had normal 12-lead electrocardiography, stress echocardiography, and routine hematology and biochemistry profiles.

DCM Subjects

Patients with DCM were prospectively identified as part of a detailed pathophysiological study assessing the effects of myocardial fibrosis on cardiac mechanics (REC: 12/WM/0157). The diagnosis of idiopathic DCM was made on the basis of left ventricular dilatation and systolic dysfunction in the absence of valvular heart disease, congenital heart disease, and ischemic heart disease sufficient to cause ventricular impairment, following gadolinium contrast-enhanced CMR (16), and normal coronary angiography.

MR Acquisition

MR studies were conducted using a 1.5-T scanner (Magnetom Avanto, Siemens, Erlangen, Germany). The time taken to acquire images for each patient was recorded.

SSFP

Vertical long axis (VLA) and horizontal long axis (HLA) SSFP cine imaging of the left and right ventricles was performed. These images were then used to pilot the LV short axis stack acquired using serial contiguous short axis cines (retrospective electrocardiographic gating, SSFP [True-FISP], temporal resolution 40–50 msec, repetition time [TR] 3.2 msec, echo time [TE] 1.7 msec, flip angle [FA] 60°, field of view [FOV] 360 mm, in-plane resolution 1.5×1.5 mm^2, slice thickness 7 mm with 3 mm gap, 25 phases per cardiac cycle) in accordance with previously validated methodology (17).

Myocardial Tagging

Three short axis tagged images at the LV base (mitral valve), middle (papillary muscle) and apex, as well as an HLA image were acquired using prospective electrocardiographic gating. A uniform tag grid was created on the images using SPAMM with a tag separation of 8 mm using a segmented *k*-space fast field echo multishot sequence (TR 3.9 msec, TE 1.7 msec, voxel size $1.99 \times 2.04 \times 8.00$ mm^3, FA 5°, tag grid angle 45° with slice thickness 8 mm, temporal resolution 30 msec, minimum 15 phases per cardiac cycle), as previously described (5). For DCM patients, tagging was performed prior to administration of gadolinium.

Myocardial Strain and Strain Rate Analysis

A timed offline analysis was performed on tagged and SSFP images at identical slice positions by two independent blinded observers (R.J.T and W.E.M.; 3 and 4 years experience, respectively). Both tagged and SSFP

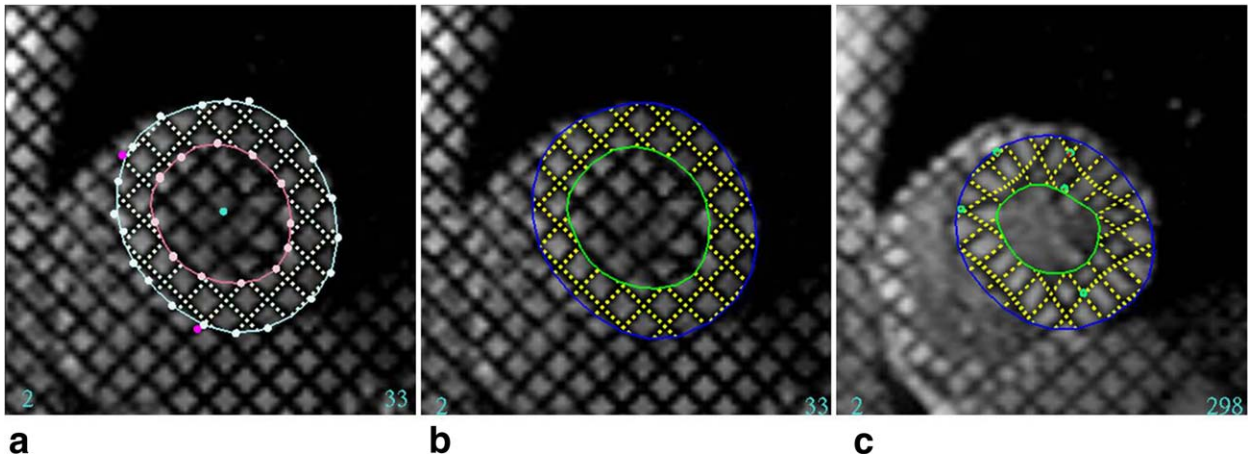

Figure 1. Overview of the generalized CIMTag2D analysis framework. **a:** Guide points placed by the user on the endocardial and epicardial border of the LV in the first frame (end-diastole) were fitted by the model using linear least squares optimization, resulting in an initial segmentation of the LV with minimal user interaction and subsequent initialization of the finite element model in the first frame of the SPAMM sequence. **b:** Visual depiction of the tissue displacement map provided by non-rigid registration image tracking process at end-diastole. **c:** User corrected texture map overlay as seen after placing guide points in end-systole, thereby interactively warping the model to provide a best fit between image tags and model stripes.

slices were reviewed by two independent experts (R.P.S and P.L.; 12 and 15 years experience, respectively) and only high-quality MR studies were included for analysis.

CIMTag Dynamic Tissue-Tagging

Tagged images were analyzed with CIMTag2D software (Cardiac Image Modelling, University of Auckland, Auckland, NZ). An overview of the generalized analysis framework is depicted in Fig. 1. The model geometry was initialized in the first frame (end-diastole) using guide-point modeling (18). Briefly, guide points placed by the user on the endocardial and epicardial border of the LV in the end-diastolic frame were fitted by the model using linear least-squares optimization, resulting in an initial segmentation of the LV with minimal user interaction (Fig. 1a). The reference model was then automatically warped to fit the tissue displacement map given by the SPAMM

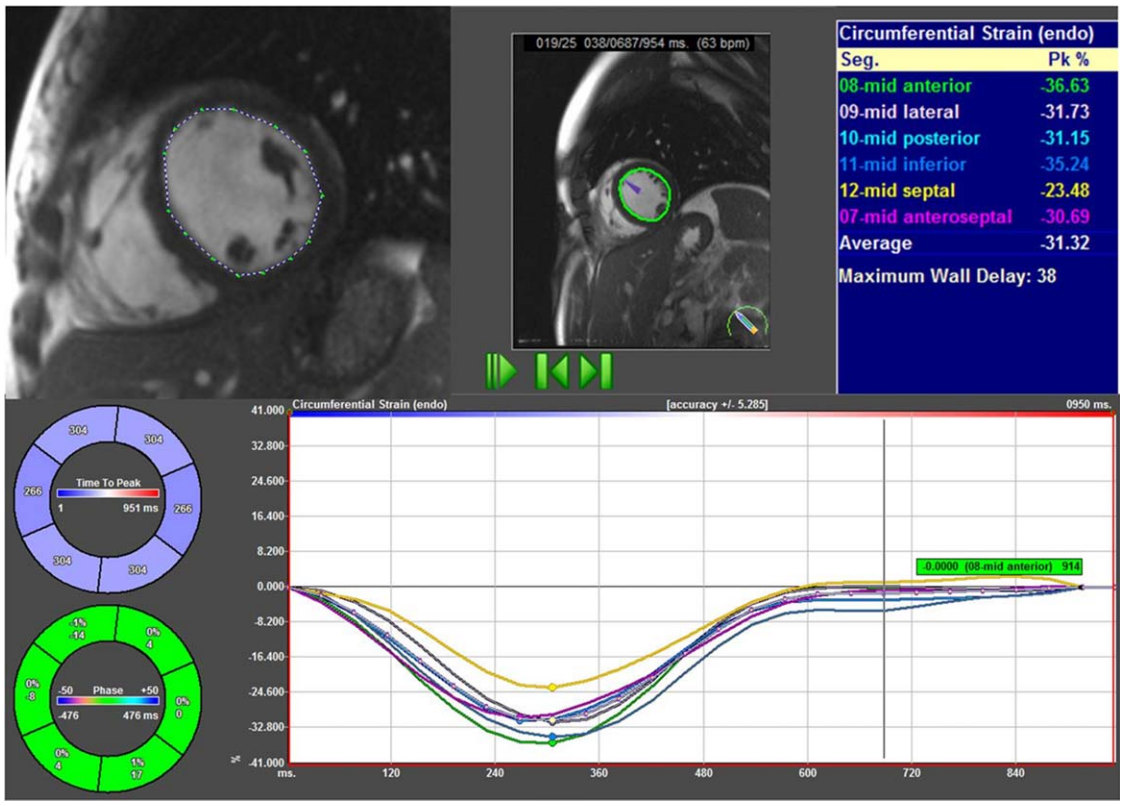

Figure 2. Acquisition of circumferential strain with FT software in a normal subject. The endocardial contour of a midventricular SSFP image is drawn manually. The first segment is always set in the anterior septum for consistency.

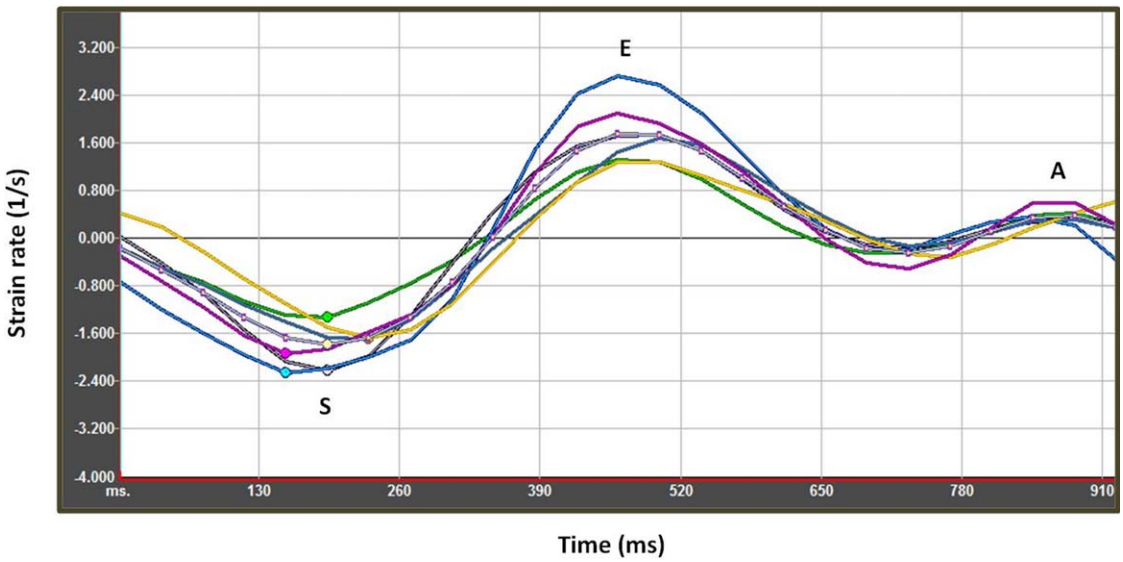

Figure 3. Representative circumferential strain rate profile from FT at the mid LV level of a normal healthy control. This example demonstrates a typical strain rate pattern with S (systolic), E (early diastolic), and A (late diastolic) waves. The dotted white line represents the global subendocardial circumferential strain rate. [Color figure can be viewed in the online issue, which is available at wileyonlinelibrary.com.]

images. The tissue displacement map was given from a nonrigid registration tracking procedure as previously described (8,19,20). Points were tracked from frame to frame using the incremental displacement maps. A texture map of model stripes was overlaid on the display (Fig. 1b) to provide a graphical representation of the tracking result. The initial tag locations, spacing, and orientation were automatically determined by interrogating the location of the harmonic peaks in the *k*-space data. The user corrected any tracking errors by placing guide points on the texture map overlay, thereby interactively warping the model to provide a best fit between image tags and model stripes (Fig. 1c). The HLA image sequence was used to determine LV longitudinal strain and SR. Left ventricular circumferential strain and SR were measured from the three short axis views. Whole wall global peak systolic strain and SR values were obtained and subdivided according to wall thickness into respective thirds: subepicardium, midwall, and subendocardium.

CMR-FT

Diogenes CMR-FT software (TomTec Imaging Systems, Munich, Germany), a vector-based analysis tool, was

Table 1
Baseline Characteristics of the Study Population

Baseline characteristics	Controls ($n = 35$)	DCM ($n = 10$)	Overall ($n = 45$)
Age (years)	41 ± 12	58 ± 14*	44 ± 14
Male gender (%)	26 (62)	6 (60)	32 (63)
Ethnicity			
Caucasian (%)	36 (90)	8 (80)	45 (88)
Asian (%)	3 (8)	1 (10)	4 (8)
Afro-Caribbean (%)	1 (2)	1 (10)	2 (4)
Weight (kg)	77 ± 11	87 ± 17*	79 ± 13
Heart rate (bpm)	66 ± 10	70 ± 10	67 ± 10
Systolic blood pressure (mmHg)	120 ± 11	112 ± 14†	119 ± 12
Diastolic blood pressure (mmHg)	72 ± 6	72 ± 11	72 ± 7
Left ventricular ejection fraction (%)	71 ± 6	33 ± 15‡	69 (64–74)§
End-diastolic volume (mL)	124 ± 25	205 ± 51‡	137 ± 43
End-systolic volume (mL)	37 ± 13	140 ± 60‡	39 (30–59)
Stroke volume (mL)	87 ± 14	64 ± 21‡	84 ± 17
Left ventricular mass (g)	122 ± 27	161 ± 21‡	123 (106–141)
Left ventricular mass index (g/m^2)	64 ± 11	82 ± 20‡	64 (59–73)
Late gadolinium enhancement result	–	All negative	–

Data are mean ± standard deviation, frequency (percentage) or median (interquartile range).
DCM, dilated cardiomyopathy
*$P < 0.01$;
†$P < 0.05$;
‡$P < 0.001$ (compared with controls using an independent two-tailed Student's *t* test).
§Range of left ventricular ejection fraction for overall cohort was 19–79%.

Table 2
Comparison of FT Versus Tagging Derived Global Strain and Strain Rate Parameters for the Overall Cohort, in Healthy Controls and in Patients With Dilated Cardiomyopathy

Healthy controls ($n = 33$)	Feature tracking	Tagging whole wall	Tagging sub-epicardium	Tagging mid wall	Tagging sub-endocardium
Long axis function (HLA)					
Peak systolic longitudinal E					
Mean value ± SD (%)	–19.5 ± 3.5	−18.0 ± 3.5	−15.9 ± 3.0	−17.7 ± 3.2	−18.0 ± 3.5
P-value*	–	0.01	<0.001	0.002	0.04
Pearson's correlation coefficient	–	0.29	0.25	0.27	0.35
P-value†	–	0.09	0.15	0.11	0.04
Bias ± SD (%)	–	2.51 ± 4.0	3.6 ± 4.0	3.6 ± 4.0	1.42 ± 4.0
Peak systolic longitudinal SR					
Mean value ± SD (1/s)	–1.12 ± 0.22	−0.95 ± 0.24	−0.90 ± 0.23	−0.97 ± 0.24	−1.03 ± 0.26
P-value*	–	0.001	<0.001	0.002	0.07
Pearson's correlation coefficient	–	0.27	0.27	0.27	0.31
P-value†	–	0.12	0.12	0.11	0.06
Bias ± SD (1/s)	–	0.17 ± 0.28	0.22 ± 0.27	0.16 ± 0.28	0.09 ± 0.28
Early diastolic longitudinal SR					
Mean value ± SD (1/s)	1.19 ± 3.5	0.69 ± 0.30	0.67 ± 0.30	0.70 ± 0.30	0.72 ± 0.30
P-value*	–	<0.001	<0.001	<0.001	<0.001
Pearson's correlation coefficient	–	0.20	0.22	0.19	0.19
P-value†	–	0.25	0.20	0.27	0.27
Bias ± SD (1/s)	–	−0.50 ± 0.40	−0.51 ± 0.40	−0.49 ± 0.40	−0.47 ± 0.40
Short axis function (mid LV)					
Peak systolic circumferential E					
Mean value ± SD (%)	–24.8 ± 2.9	−18.6 ± 2.5	−12.9 ± 2.0	−18.3 ± 2.6	−24.9 ± 3.0
P-value*	–	<0.001	<0.001	<0.001	0.90
Pearson's correlation coefficient	–	0.15	0.02	0.10	0.26
P-value†	–	0.39	0.92	0.55	0.13
Bias ± SD (%)	–	6.2 ± 3.5	11.9 ± 3.5	6.6 ± 3.7	−0.08 ± 4.0
Peak systolic circumferential SR					
Mean value ± SD (1/s)	–1.48 ± 0.27	−1.01 ± 0.18	−0.72 ± 0.13	−0.98 ± 0.18	−1.34 ± 0.31
P-value*	–	<0.001	<0.001	<0.001	0.02
Pearson's correlation coefficient	–	0.22	0.01	0.18	0.28
P-value†	–	0.21	0.99	0.31	0.09
Bias ± SD (1/s)	–	0.48 ± 0.29	0.76 ± 0.30	0.50 ± 0.30	0.14 ± 0.06
Early diastolic circumferential SR					
Mean value ± SD (1/s)	1.34 ± 0.32	0.79 ± 0.16	0.48 ± 0.11	0.76 ± 0.16	1.15 ± 0.24
P-value*	–	<0.001	<0.001	<0.001	0.001
Pearson's correlation coefficient	–	0.53	0.44	0.52	0.45
P-value†	–	0.001	<0.01	0.001	<0.01
Bias ± SD (1/s)	–	−0.55 ± 0.27	−0.85 ± 0.29	−0.58 ± 0.28	−0.19 ± 0.30

Dilated cardiomyopathy ($n = 10$)	Feature tracking	Tagging whole wall	Tagging sub-epicardium	Tagging mid wall	Tagging sub-endocardium
Long axis function (HLA)					
Peak systolic longitudinal E					
Mean value ± SD (%)	–9.7 ± 4.7	−8.2 ± 3.5	−7.6 ± 3.0	−8.3 ± 3.6	−8.8 ± 3.9
P-value*	–	0.26	0.16	0.30	0.44
Pearson's correlation coefficient	–	0.77	0.73	0.75	0.80
P-value†	–	0.08	0.10	0.09	0.05
Bias ± SD (%)	–	1.5 ± 2.9	2.1 ± 3.1	1.4 ± 3.0	0.9 ± 2.7
Peak systolic longitudinal SR					
Mean value ± SD (1/s)	–0.56 ± 0.19	−0.45 ± 0.19	−0.46 ± 0.15	−0.46 ± 0.19	−0.47 ± 0.23
P-value*	–	0.04	0.16	0.05	0.08
Pearson's correlation coefficient	–	0.88	0.65	0.87	0.91
P-value†	–	0.02	0.16	0.03	0.01
Bias ± SD (1/s)	–	0.11 ± 0.10	0.10 ± 0.15	0.10 ± 0.10	0.09 ± 0.10
Early diastolic longitudinal SR					
Mean value ± SD (1/s)	0.49 ± 0.20	0.31 ± 0.22	0.28 ± 0.18	0.31 ± 0.23	0.35 ± 0.26
P-value*	–	0.07	0.05	0.07	0.17
Pearson's correlation coefficient	–	0.57	0.45	0.59	0.60
P-value†	–	0.24	0.38	0.22	0.21
Bias ± SD (1/s)	–	−0.19 ± 0.20	−0.22 ± 0.20	−0.19 ± 0.19	−0.14 ± 0.22

Table 2. *Continued*

Dilated cardiomyopathy ($n = 10$)	Feature tracking	Tagging whole wall	Tagging sub-epicardium	Tagging mid wall	Tagging sub-endocardium
Short axis function (mid LV)					
Peak systolic circumferential E					
Mean value ± SD (%)	–9.6 ± 4.8	−7.2 ± 2.4	−6.3 ± 1.8	−7.2 ± 2.2	−8.1 ± 1.9
P-value*	–	0.15	0.07	0.15	0.36
Pearson's correlation coefficient	–	0.70	0.76	0.73	0.61
P-value†	–	0.12	0.08	0.10	0.20
Bias ± SD (%)	–	2.5 ± 3.5	3.3 ± 3.6	2.4 ± 3.5	1.6 ± 3.8
Peak systolic circumferential SR					
Mean value ± SD (1/s)	–0.57 ± 0.23	−0.41 ± 0.10	−0.36 ± 0.09	−0.40 ± 0.10	−0.50 ± 0.23
P-value*	–	0.06	0.04	0.05	0.37
Pearson's correlation coefficient	–	0.80	0.67	0.82	0.73
P-value†	–	0.06	0.14	<0.05	0.10
Bias ± SD (1/s)	–	0.16 ± 0.17	0.20 ± 0.19	0.17 ± 0.16	0.07 ± 0.17
Early diastolic circumferential SR					
Mean value ± SD (1/s)	0.48 ± 0.26	0.46 ± 0.20	0.30 ± 0.13	0.44 ± 0.20	0.63 ± 0.26
P-value*	–	0.89	0.23	0.79	0.41
Pearson's correlation coefficient	–	0.18	0.20	0.20	0.20
P-value†	–	0.73	0.71	0.71	0.71
Bias ± SD (1/s)	–	−0.03 ± 0.36	−0.18 ± 0.32	−0.04 ± 0.36	0.15 ± 0.41

E, Lagrangian strain; HLA, horizontal long axis; LV,left ventricle; SD, standard deviation; SR, strain rate
*Feature tracking derived means compared with tagging measurements using a paired Student's *t* test.
†Using Pearson's *r*, correlation coefficient.

used to perform subendocardial strain analysis in the corresponding SSFP images (Fig. 2). Endocardial borders were drawn manually in the end-diastolic frame for each image. The CMR-FT software automatically propagated the contour and followed its features (brightness gradient at the tissue–cavity interface, dishomogeneities of the tissue, spatial coherence) throughout the remainder of the cardiac cycle. Global measures of subendocardial longitudinal strain were derived from the HLA view. Global subendocardial circumferential strain parameters were derived from the three short axis views. As for tagging analysis, global diastolic SR signals were recorded during early filling (Fig. 3). CMR-FT segmental strain parameters were not extracted for comparison with tagging because a series of reports including our own substudy of patients with ischemic cardiomyopathy (Supporting Materials, Appendix A) demonstrate high intra- and interobserver variability for regional data (11–13,21).

Left Ventricular Function, Volumes, Mass, and Wall Thickness

Analysis of LV function, volume and LV mass was performed offline (Argus Software, Siemens, Erlangen, Germany) in accordance with previously validated methodologies (17). Left ventricular mass was indexed to body surface area using the Mosteller formula: BSA (m^2) = $\sqrt{}$((weight (kg)×height (cm))/3600). Left ventricular wall thickness was measured in the short axis in each of the six segments of the mid-LV according to the AHA standardized model, and at the identical slice position from which mid LV circumferential strain parameters were derived.

Statistical Analysis

Data are presented as mean ± standard deviation, median (interquartile range), or frequency (percentage). Data distribution for continuous variables was assessed using normality plots and the Kolmogorov–Smirnov test. Nonparametric data were log-transformed prior to analysis to achieve normality. Individual strain and SR values obtained using the two different methods were compared using the Bland–Altman technique and Pearson's correlation. A Spearman's rank correlation of the differences with

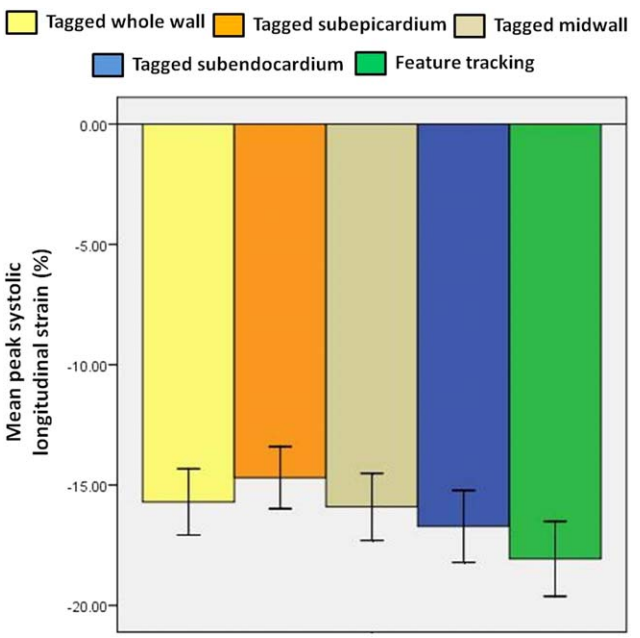

Figure 4. Global longitudinal strain measures calculated from FT and a targeted tagging analysis across the three layers of the myocardium. When using an ANOVA with repeated measures with a Greenhouse-Geisser correction, the mean scores for peak systolic global longitudinal strain across the three layers of the myocardium were statistically different ($F(1.2, 49.9) = 54.8$, $P < 0.001$). [Color figure can be viewed in the online issue, which is available at wileyonlinelibrary.com.]

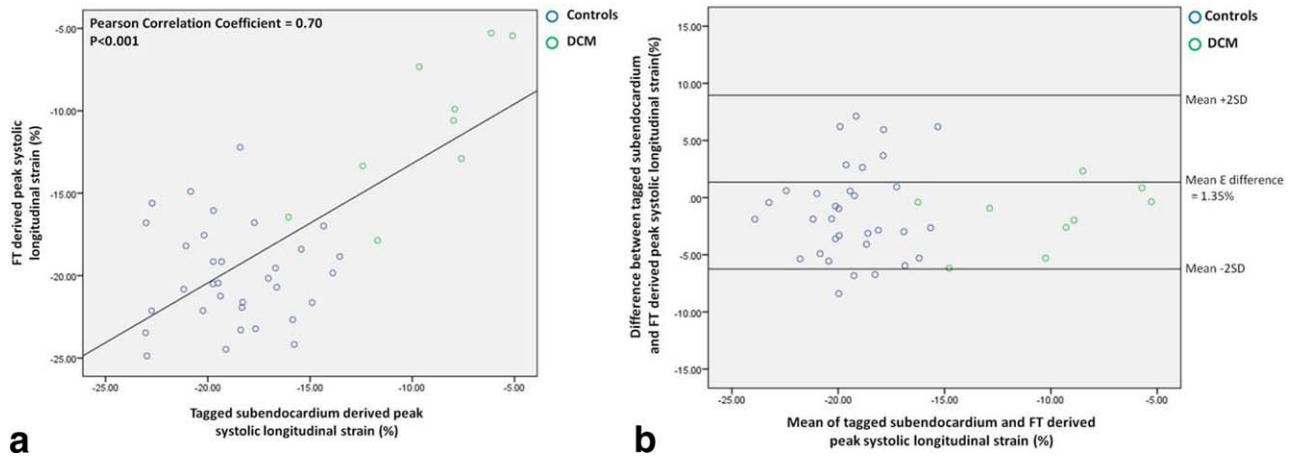

Figure 5. (a) Pearson correlation and (b) Bland Altman plots demonstrating agreement for peak systolic global longitudinal strain calculation using FT versus tagging. Spearman's rank correlation of the differences and the means was nonsignificant ($\rho = 0.078$, $P = 0.625$). [Color figure can be viewed in the online issue, which is available at wileyonlinelibrary.com.]

the means of parameters derived from FT and CIMTag was performed. The mean strain parameters derived from the two techniques were compared using paired *t*-tests if normally distributed. Continuous variables from controls and DCM patients were compared using independent *t*-tests. An analysis of variance (ANOVA) with repeated measures with a Greenhouse-Geisser correction was used to compare differences in tagging derived strain parameters across the three myocardial layers. Statistical analysis was performed using SPSS v. 21 (Chicago, IL). A type I error rate <5% ($P < 0.05$) was considered statistically significant.

Variability of CIMTag2D and CMR-FT Strain Measurements

Interobserver and intraobserver variability assessments were performed using a paired *t*-test and reported as a bias (mean difference) and standard deviation (SD). The coefficient of variability, defined as the SD of the differences divided by their mean, and intraclass correlation coefficient (ICC) for absolute agreement were also calculated (22).

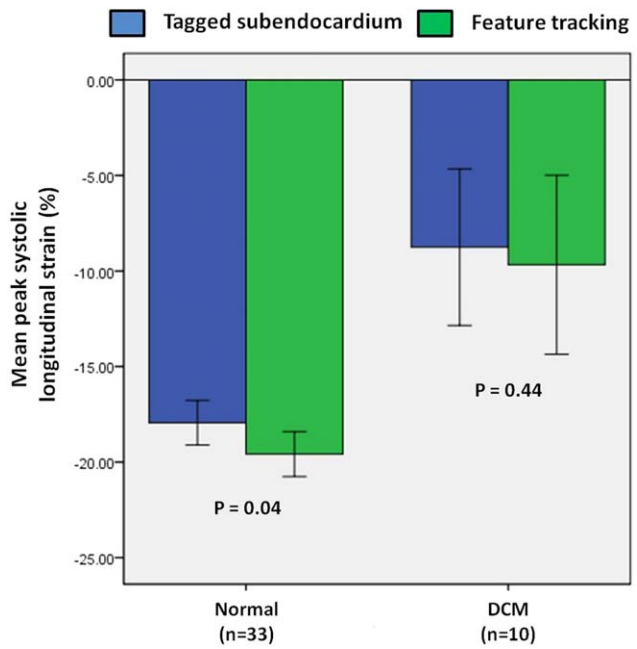

Figure 6. Comparison of CIMTag versus FT-derived peak systolic global longitudinal strain between control and DCM subjects. [Color figure can be viewed in the online issue, which is available at wileyonlinelibrary.com.]

RESULTS

Study Population

A total of 45 subjects were identified (35 controls, 10 DCM); age was 44 ± 14 years. Baseline characteristics are shown in Table 1. Compared with healthy controls, DCM patients were older (58 ± 14 vs. 41 ± 12 years, $P < 0.01$) and had higher body weight (87 ± 17 vs. 77 ± 11 kg, $P < 0.01$). No other demographic data were significantly different.

All participants completed the full imaging protocol. Two controls, however, were excluded from the imaging analysis because of poor tagging imaging quality due to breathing artifacts ($n = 1$) and electrocardiogram gating issues ($n = 1$); these participants were therefore only included in volumetric and left ventricular mass assessments. All SSFP images were of excellent image quality and compatible with CMR-FT software.

Myocardial Strain and Strain Rate Analysis

A detailed summary of the statistical comparison of FT versus tagging for all global strain and strain rate parameters is presented in Table 2.

Long Axis Function

Global Longitudinal Strain (E_{ll})

Tagged imaging revealed a transmural longitudinal strain gradient; there was a progressive increase in longitudinal deformation from the subepicardium through the midwall and into the subendocardium ($P < 0.001$; Fig. 4). In an analysis of all subjects, CMR-FT peak systolic global longitudinal strain (E_{ll}) correlated most strongly with CIMTag E_{ll} values derived from tagging of the subendocardium ($r = 0.70$, $P < 0.001$; Fig. 5a). A Bland–Altman plot (Fig. 5b) demonstrates agreement but with a small systematic overestimation from CMR-FT

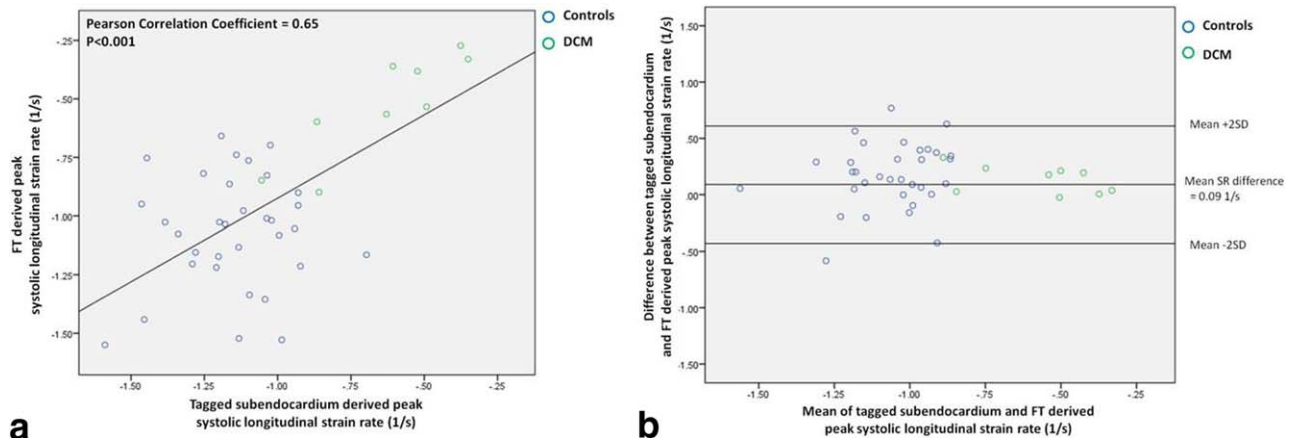

Figure 7. (a) Pearson correlation and (b) Bland Altman plots demonstrating agreement for peak systolic global longitudinal strain rate calculation using FT versus tagging. Spearman's rank correlation of the differences and the means was nonsignificant ($\rho = 0.196$, $P = 0.213$). [Color figure can be viewed in the online issue, which is available at wileyonlinelibrary.com.]

(−18.1 ± 5.0% vs. −16.7 ± 4.8%, bias 1.3 ± 3.8%, $P = 0.03$). While in DCM patients the mean peak global E_{ll} values were not significantly different between the two techniques (−9.7 ± 4.5% vs. −8.8 ± 3.9%, $P = 0.44$), among healthy controls there was a small but significant difference in E_{ll} values derived from CMR-FT versus tagged imaging (−19.5 ± 3.5% vs. −18.0 ± 3.5%, $P = 0.04$; Fig. 6).

Longitudinal Strain Rate

The subendocardial layer also had the highest values for peak systolic longitudinal SR derived from tagging (Table 2). Among all participants, FT-peak systolic global longitudinal SR correlated with corresponding CIMTag derived measurements from the subendocardium ($r = 0.65$, $P < 0.001$; Fig. 7a). There was agreement between the two techniques for peak systolic global longitudinal SR values with a small tendency towards higher values from CMR-FT compared with tagging (−1.04 ± 0.29 1/s vs. −0.95 ± 0.32 1/s, bias 0.09 ± 0.26 1/s, $P = 0.04$; Fig. 7b). Although the correlation remained significant ($r = 0.42$, $P = 0.007$), the weakest agreement between the two techniques was for early diastolic global longitudinal SR (1.10 ± 0.40 1/s vs. 0.67 ± 0.32 1/s, bias −0.42 ± 0.40 1/s, $P < 0.001$; Fig. 8).

Short Axis Function

Circumferential Strain (E_{cc})

Across all subjects, CMR-FT derived peak systolic global circumferential strain measurements at the mid LV slice were not significantly different from those calculated via tagging (Fig. 9). As with the long axis analysis, FT–E_{cc} values correlated most strongly with CIMTag-E_{cc} values derived from the subendocardium ($r = 0.83$, $P < 0.001$; Fig. 10a and 11). A Bland–Altman plot shows close agreement between the two techniques across the entire cohort with neither systemic overestimation nor underestimation and a bias of only 0.2 ± 4.0% (−22.7 ± 6.2% vs. −22.5 ± 6.9%, $P = 0.80$; Fig. 10b).

Measures of circumferential strain from the mid-LV slice showed better agreement between CMR-FT and CIMTag compared with measures derived from the LV base and apex (Supporting Materials, Appendix B). Tagged imaging also showed a graded increase in

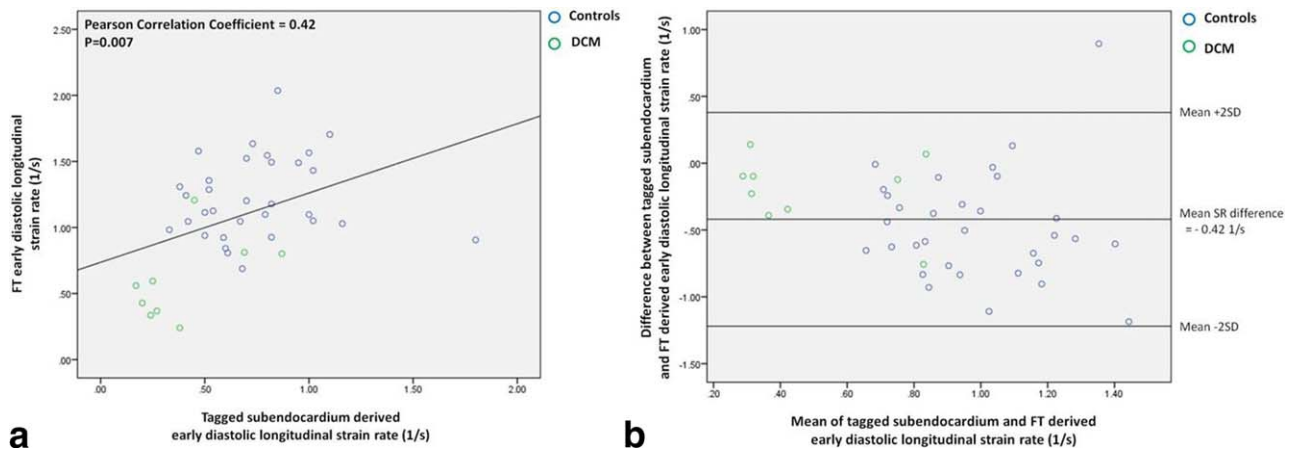

Figure 8. (a) Pearson correlation and (b) Bland–Altman plots demonstrating agreement for early diastolic global longitudinal strain rate calculation using FT versus tagging. Spearman's rank correlation of the differences and the means was significant ($\rho = -0.329$, $P = 0.036$), suggesting a proportional error with a downward trend. [Color figure can be viewed in the online issue, which is available at wileyonlinelibrary.com.]

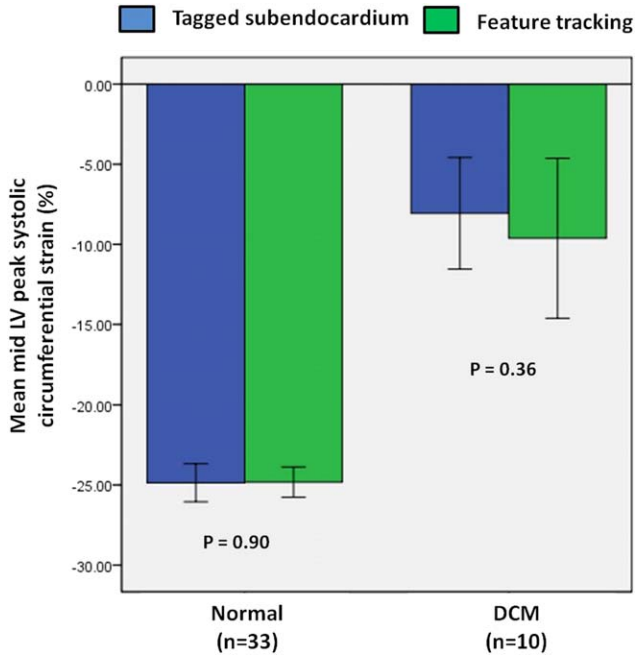

Figure 9. Comparison of CIMTag versus FT-derived peak systolic global circumferential strain between control and DCM subjects. [Color figure can be viewed in the online issue, which is available at wileyonlinelibrary.com.]

circumferential shortening from the base towards the apex.

Circumferential Strain Rate

Among all participants, FT-peak systolic global circumferential SR correlated closely with corresponding CIMTag derived measurements from the subendocardium ($r = 0.69$, $P < 0.001$; Fig. 12a). As for longitudinal SR, Bland–Altman analysis also showed agreement between the two techniques for calculation of peak systolic global circumferential SR (−1.35 ± 0.42 1/s vs. −1.22 ± 0.42 1/s, bias 0.13 ± 0.33 1/s; Fig. 12b). FT-early diastolic global circumferential SR also correlated with tagging derived values from the subendocardium ($r = 0.64$, $P < 0.001$; Fig. 13a) and showed satisfactory agreement (1.21 ± 0.44 vs. 1.07 ± 0.30, bias −0.14 ± 0.34 1/s; Fig. 13b).

Time Taken for Image Acquisition and Offline Analysis

Table 3 shows the large difference in postprocessing time taken between the two techniques (5.9 ± 0.8 vs. 23.2 ± 3.5 min, $P < 0.001$).

Agreement Between CMR-FT and Tagging as a Function of Ventricular Wall Thickness

There was no significant difference between the mid-LV ventricular wall thickness of DCM patients and healthy controls (7.2 ± 1.1 mm vs. 7.3 ± 1.0 mm, $P = 0.7$). The limits of agreement (LoA) for calculation of peak systolic circumferential strain in patients with DCM versus healthy controls were comparable (LoA −7.76 to 7.92% vs. −5.85 to 9.05%). For calculation of peak systolic circumferential strain across the overall cohort, there was no association between ventricular wall thickness and the size of the bias relative to its mean value ($r = -0.15$, $P = 0.33$).

Inter- and Intraobserver Variability

Intraobserver and interobserver variability for CMR-FT analysis of peak systolic global longitudinal strain was small (bias −0.49 ± 1.83% and 0.22 ± 1.13%; respectively). The reproducibility of CMR-FT strain measurements compared favorably with CIMTag, particularly with respect to interobserver variability (Tables (4 and 5)).

DISCUSSION

In this study we principally compared a SSFP FT-based algorithm against a reference standard tagged image analysis (SPAMM) for the assessment of Lagrangian strain and SR. This report builds upon recent validation work by including comparisons of 2D longitudinal and circumferential strain and SR during systole *and* diastole; only systolic strain parameters have previously been validated (10,14,15). We compared the ability of the two techniques to accurately measure diastolic SR during early filling, a sensitive marker of LV diastolic dysfunction which is an important precursor of incident heart failure (23).

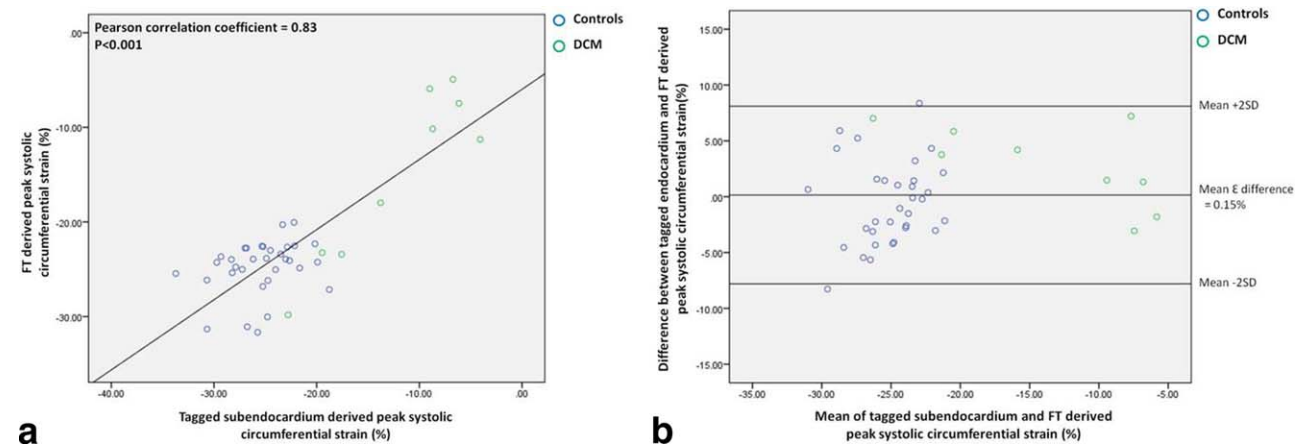

Figure 10. (a) Pearson correlation and (b) Bland–Altman plots demonstrating agreement for peak systolic global circumferential strain calculation using FT versus tagging. Spearman's rank correlation of the differences and the means was nonsignificant ($\rho = 0.292$, $P = 0.06$). [Color figure can be viewed in the online issue, which is available at wileyonlinelibrary.com.]

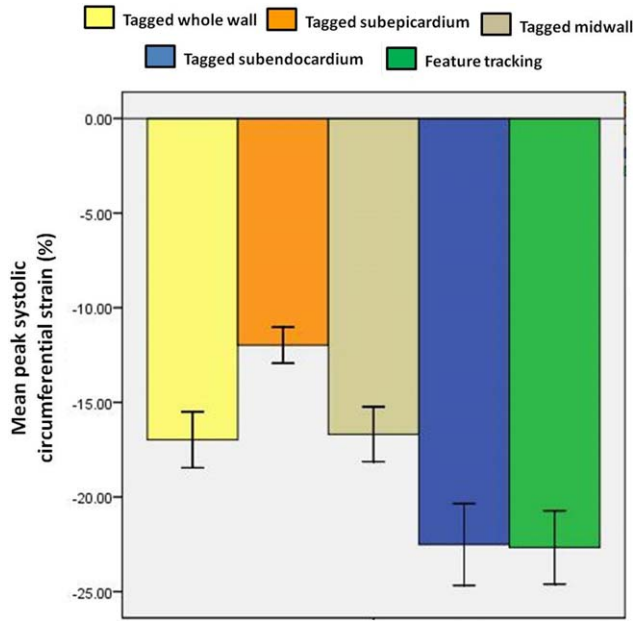

Figure 11. Global circumferential strain measures calculated from feature tracking and a targeted tagging analysis across the three layers of the myocardium. Using an ANOVA with repeated measures with a Greenhouse-Geisser correction, the mean scores for peak systolic global circumferential strain across the myocardium were statistically different ($F(1.0, 41.8) = 218.4$, $P < 0.001$). [Color figure can be viewed in the online issue, which is available at wileyonlinelibrary.com.]

On the basis of our analysis performed in the subendocardium and in the circumferential direction, CMR-FT could realistically be extended to the computation of early diastolic strain rate. From a technical viewpoint, the current study benefits from having performed all sequences on a 1.5T MR scanner; a previous validation utilized a mix of acquisitions from 1.5T and 3T MR scanners (10). The validation described herein was also undertaken on corresponding SSFP and tagging images acquired from identical slice positions, a method which has not always been adopted (10). Finally, by performing a timed analysis this report highlights that CMR-FT can generate strain data over four times more rapidly than myocardial tagging and this has obvious clinical implications.

Our results contrast with a recent report from Augustine *et al.* (15) which demonstrated that CMR-FT measurements of longitudinally directed strain showed poor agreement with tagging. There are a number of differences between the studies which could account for this discrepancy. In our analysis, strain parameters derived from CMR-FT versus tagging were compared for all patients entered into the study, which included healthy subjects as well as those with DCM; the validation by Augustine *et al.* was more modest and included only 20 healthy volunteers out of a total of 145 subjects (13.8%). Moreover, Augustine *et al.* compared measurements of longitudinal strain derived from tagging across the whole myocardial wall with CMR-FT measures derived from the blood–tissue interface, which effectively select subendocardial deformation information. In order to perform a valid comparison between the two techniques, it is imperative to measure strain from the equivalent myocardial layer, namely, the subendocardium. Indeed, the longitudinal myocardial fibers are principally located in the subendocardium (24). For this reason, in our Bland–Altman analyses we made the *a priori* decision to compare CMR-FT strain parameters with tagged subendocardial values, which likely explains the improved agreement between the two techniques reported in the current study.

Results of the two methods for calculation of subendocardial strain measures correlate and, with the exception of early diastolic longitudinal SR, Bland–Altman assessments display good agreement, although there remain small differences in the measurements between techniques. Some of the variability in CIMTag strain measurements may relate to the requirement to manually contour both endocardial and epicardial borders, together with the need to make a visual assessment of the tissue displacement map before making corrections to provide a best fit between image tags and model stripes. In contrast, only endocardial contours were constructed in the CMR-FT platform in this study, after which the process was fully automated without an option to modify tracking. These

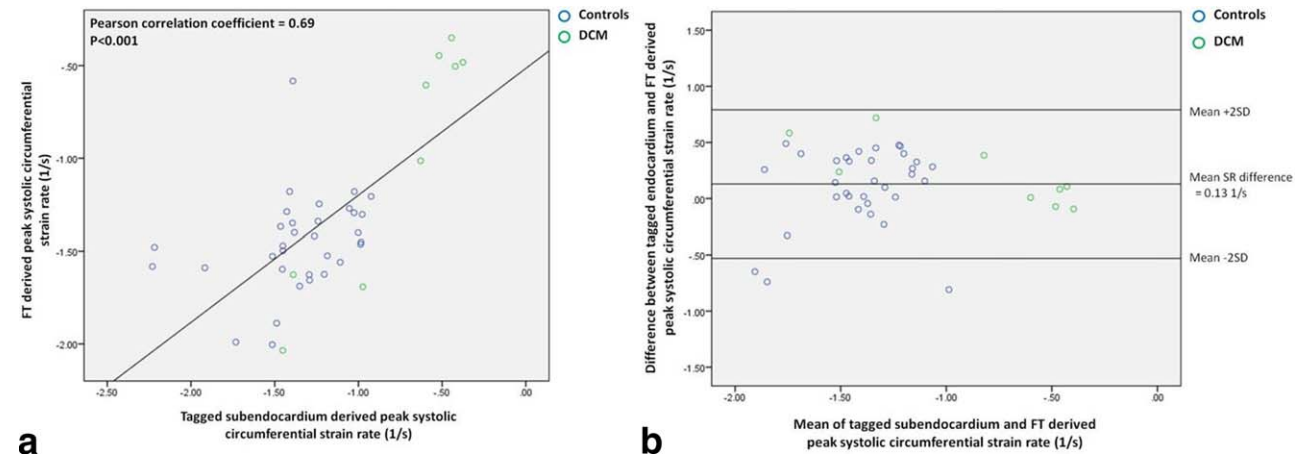

Figure 12. (a) Pearson correlation and (b) Bland–Altman plots demonstrating agreement for peak systolic global circumferential strain rate calculation using FT versus tagging. Spearman's rank correlation of the differences and the means was nonsignificant ($\rho = -0.034$, $P = 0.833$). [Color figure can be viewed in the online issue, which is available at wileyonlinelibrary.com.]

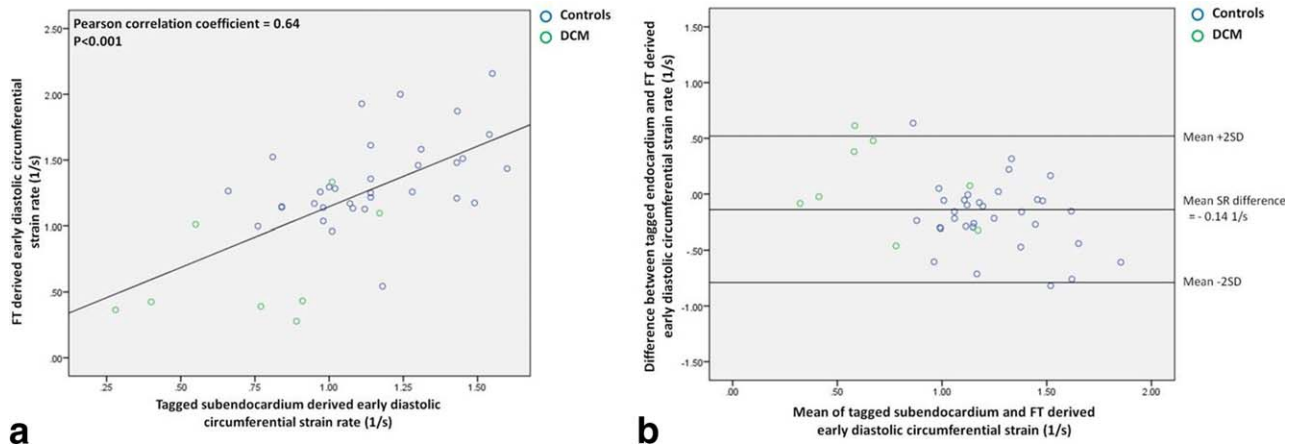

Figure 13. (a) Pearson correlation and (b) Bland–Altman plots demonstrating agreement for early diastolic global circumferential strain rate calculation using FT versus tagging. Spearman's rank correlation of the differences and the means was significant ($\rho = -0.315$, $P = 0.045$), suggesting a proportional error with a downwards trend. [Color figure can be viewed in the online issue, which is available at wileyonlinelibrary.com.]

differences may account for CIMTag measurements having poorer interobserver variability compared with CMR-FT as well as tagging postprocessing taking considerably longer. Another disadvantage of SPAMM tagging, which may also contribute to increased variability in strain outputs, is the potential for image quality to be affected by changes in heart rate. Furthermore, measurement of strain throughout the cardiac cycle to include diastolic parameters is not always achievable with 1.5T CMR scanners because of loss of tags caused by T_1 relaxation (25). CMR-FT offers a potentially more robust calculation of diastolic strain data because it relies on standard cine images whose spatial resolution is not adversely affected by T_1 relaxation.

In general, the CMR-FT derived longitudinal strain and SR data were more variable than the circumferential data calculated from the short axis. This may be due to difficulty tracking at the blood–tissue interface and a tendency to track the mitral valve apparatus. In keeping with previous reports, circumferential strain showed the strongest agreement between the two techniques and was particularly robust for the mid-LV slice (10,15). At the LV apex, however, less muscle is available for creating the tag grid upon which the guide point modeling for CIMTag is based, which may have led to increased variability. CMR-FT may lose some of its ability to track the features in each voxel at the tissue–cavity interface at the apex (where there is a potential for cavity obliteration in end-systole) which may also account for increased error. The variability in circumferential strain at the LV base could be explained by a relative increase in the through-plane motion typically observed at this level. The extent to which this degree of variability in CMR-FT measurements might relate to clinical use requires further exploration.

This study confirmed a transmural strain gradient which exists across the myocardial wall (26); both longitudinal and circumferential strain values from tagging increased from subepicardial through to subendocardial layers. This likely explains the better agreement of CMR-FT with tagging values from the subendocardium. It also offers a potential explanation for the reduced sensitivity and slightly higher strain values derived from CMR-FT. The CMR-FT algorithm only tracked deformation at the endocardial border, therefore potentially losing important transmural information captured in tag grids that span the entire thickness of the ventricular wall. Mechanistically, this is in keeping with the pathology of dilated cardiomyopathy, which is characterized by epicardial injury on *ex vivo* histopathology and demonstrable *in vivo* with late postgadolinium imaging (27). In this study, ventricular wall thickness was not significantly different between DCM and controls. In DCM, the ventricles are dilated but often with normal ventricular wall thickness, imparting an appearance of thin ventricular walls (28). Nonetheless, in an analysis which included all study subjects, wall thickness did not appear to affect the agreement between strain measures calculated using CMR-FT and myocardial tagging.

There is already evidence that regional assessment by CMR-FT may not be as robust as existing tagging modalities but the potential advantages in ease of acquisition and reduced time for analysis suggest that this method of assessing global deformation could still be of clinical utility. By design, this study did not attempt to validate regional measures because of ongoing concerns over the reproducibility of CMR-FT segmental data (11–13). CMR-FT applies 2D B-mode tracking such that the motion components parallel to

Table 3
Time Taken for Image Acquisition and Postprocessing Analysis

	Feature tracking	Tagging
SSFP acquisition time (min)	12.1 ± 3.4	12.1 ± 3.4
SPAMM acquisition time (min)	–	8.4 ± 2.3
Post-processing time (min)	5.9 ± 0.8*	23.2 ± 3.5

Data are mean ± SD. SSFP, steady-state free precession; SPAMM, spatial modulation of magnetization.
*$P < 0.001$ (means compared using a paired Student's *t* test).

Table 4
Intraobserver and Interobserver Variability for Feature Tracking Derived Global Strain Parameters

Parameter	Variability	Bias ± SD	*P* value	Limits of agreement	Coefficient of variation (%)	Intraclass correlation coefficient (95% CI)
E_{ll} (%)	Intraobserver	−0.49 ± 1.83	0.29	−4.08 to 3.11	7.68	0.88 (0.72 to 0.96)
	Interobserver	0.22 ± 1.13	0.42	−1.99 to 2.42	5.48	0.98 (0.94 to 0.99)
SSR_{ll} (1/s)	Intraobserver	0.02 ± 0.18	0.70	−0.34 to 0.38	17.89	0.89 (0.72 to 0.96)
	Interobserver	0.02 ± 0.16	0.61	−0.30 to 0.33	12.95	0.86 (0.67 to 0.95)
DSR_{ll} (1/s)	Intraobserver	0.05 ± 0.18	0.27	−0.30 to 0.40	14.84	0.85 (0.64 to 0.94)
	Interobserver	0.01 ± 0.28	0.90	−0.53 to 0.55	20.99	0.85 (0.63 to 0.94)
E_{cc} (%)	Intraobserver	−0.34 ± 0.87	0.09	−2.05 to 1.36	3.55	0.96 (0.90 to 0.99)
	Interobserver	0.63 ± 1.29	0.06	−1.90 to 3.16	4.95	0.93 (0.81 to 0.97)
SSR_{cc} (1/s)	Intraobserver	−0.02 ± 0.08	0.21	−0.18 to 0.13	5.36	0.96 (0.90 to 0.98)
	Interobserver	0.02 ± 0.11	0.56	−0.20 to 0.23	6.68	0.94 (0.84 to 0.98)
DSR_{cc} (1/s)	Intraobserver	0.00 ± 0.07	0.92	−0.13 to 0.13	5.29	0.97 (0.93 to 0.99)
	Interobserver	−0.01 ± 0.11	0.63	−0.24 to 0.21	7.82	0.96 (0.89 to 0.98)

E_{cc}, Peak systolic global circumferential strain; E_{ll}, Peak systolic global longitudinal strain; SSR_{cc}, Peak systolic global circumferential strain rate; SSR_{ll}, Peak systolic global longitudinal strain rate; DSR_{cc}, Early diastolic circumferential strain rate; DSR_{ll}, Early diastolic longitudinal strain rate.

tissue boundaries responsible for segmental information are much more affected by noise compared to the perpendicular components from which global strain measures are derived. This relates to the gradients in backscatter amplitude being much higher between tissue and blood than within the myocardium.

A number of limitations to this study deserve mention. There were a comparatively low number of subjects included with pathology; however, this cohort enabled a validated assessment of the CMR-FT based technique over a broad range of LV function. Only subendocardial global measures of deformation could be measured on CMR-FT and a comprehensive assessment of SR during late diastolic filling was not possible because of constraints over temporal resolution and loss of tags. Assessment of myocardial deformation by strain and strain rate is sensitive to differences in sampling rate. Even though considerable effort was made to ensure all tagging sequences were acquired with more than 15 phases (and many over 20 phases), there will almost inevitably be a difference in temporal resolution between a prospectively gated sequence and retrospectively gated sequence, specifically when confined by the resting heart rate and breath-holding of the patient. The issue of temporal resolution is such that while the results may correlate, values recorded are unlikely to be the same—in a clinical situation, it would be important to compare results using the same method in any single patient. All scans were performed on a 1.5T scanner for consistency, although employing a 3T scanner may have resulted in improved tag persistence. Finally, differences in breath-hold requirements may have contributed to variability between acquisitions.

In conclusion, in a study population with a wide range of LV function, CMR-FT systolic and diastolic global circumferential strain measures and systolic global longitudinal strain measures showed satisfactory agreement and correlated with corresponding values from tagged imaging. The CMR-FT global algorithm has potential for clinical utility, for it can be performed without the need for additional imaging and lengthy postprocessing. Segmental analysis, however, may benefit from further development to improve variability in regional deformation measures. In this regard, CMR-FT cannot yet be used as a robust alternative to myocardial tagging.

Table 5
Intraobserver and Interobserver Variability for Myocardial Tagging Derived Global Strain Parameters

Parameter	Variability	Bias ± SD	*P* value	Limits of agreement	Coefficient of variation (%)	Intraclass correlation coefficient (95% CI)
E_{ll} (%)	Intraobserver	−0.47 ± 0.62	0.04	−1.68 to 0.74	3.41	0.97 (0.83 to 0.99)
	Interobserver	−0.47 ± 2.02	0.49	−4.42 to 3.49	11.44	0.75 (0.29 to 0.93)
SSR_{ll} (1/s)	Intraobserver	0.00 ± 0.06	0.91	−0.11 to 0.11	6.64	1.00 (0.98 to 1.00)
	Interobserver	−0.01 ± 0.17	0.90	−0.33 to 0.32	17.27	0.60 (−0.04 to 0.89)
DSR_{ll} (1/s)	Intraobserver	0.05 ± 0.10	0.14	−0.14 to 0.24	14.15	0.89 (0.62 to 0.97)
	Interobserver	0.11 ± 0.20	0.12	−0.28 to 0.49	31.59	0.45 (−0.11 to 0.82)
E_{cc} (%)	Intraobserver	−0.39 ± 1.22	0.39	−2.79 to 2.09	4.79	0.92 (0.74 to 0.98)
	Interobserver	−0.53 ± 1.53	0.30	−3.54 to 2.48	6.01	0.86 (0.56 to 0.96)
SSR_{cc} (1/s)	Intraobserver	0.00 ± 0.06	0.92	−0.12 to 0.12	4.63	0.95 (0.82 to 0.99)
	Interobserver	−0.02 ± 0.18	0.71	−0.37 to 0.33	13.86	0.46 (−0.25 to 0.83)
DSR_{cc} (1/s)	Intraobserver	0.03 ± 0.08	0.25	−0.13 to 0.19	7.38	0.95 (0.81 to 0.99)
	Interobserver	0.09 ± 0.19	0.15	−0.27 to 0.46	16.75	0.78 (0.36 to 0.94)

E_{cc}, Peak systolic global circumferential strain; E_{ll}, Peak systolic global longitudinal strain; SSR_{cc}, Peak systolic global circumferential strain rate; SSR_{ll}, Peak systolic global longitudinal strain rate; DSR_{cc}, Early diastolic circumferential strain rate; DSR_{ll}, Early diastolic longitudinal strain rate.

ACKNOWLEDGMENT

We thank Dr. Peter Nightingale for statistical support.

REFERENCES

1. Mor-Avi V, Lang RM, Badano LP, et al. Current and evolving echocardiographic techniques for the quantitative evaluation of cardiac mechanics: ASE/EAE consensus statement on methodology and indications endorsed by the Japanese Society of Echocardiography. J Am Soc Echocardiogr 2011;24:277–313.
2. Poterucha JT, Kutty S, Lindquist RK, Li L, Eidem BW. Changes in left ventricular longitudinal strain with anthracycline chemotherapy in adolescents precede subsequent decreased left ventricular ejection fraction. J Am Soc Echocardiogr 2012;25:733–740.
3. Hankiewicz JH, Goldspink PH, Buttrick PM, Lewandowski ED. Principal strain changes precede ventricular wall thinning during transition to heart failure in a mouse model of dilated cardiomyopathy. Am J Physiol Heart Circ Physiol 2008;294:H330–336.
4. Donal E, Mascle S, Brunet A, et al. Prediction of left ventricular ejection fraction 6 months after surgical correction of organic mitral regurgitation: the value of exercise echocardiography and deformation imaging. Eur Heart J Cardiovasc Imaging 2012;13: 922–930.
5. Edwards NC, Ferro CJ, Kirkwood H, et al. Effect of spironolactone on left ventricular systolic and diastolic function in patients with early stage chronic kidney disease. Am J Cardiol 2010;106:1505–1511.
6. Yeon SB, Reichek N, Tallant BA, et al. Validation of in vivo myocardial strain measurement by magnetic resonance tagging with sonomicrometry. J Am Coll Cardiol 2001;38:555–561.
7. Young AA, Axel L, Dougherty L, Bogen DK, Parenteau CS. Validation of tagging with MR imaging to estimate material deformation. Radiology 1993;188:101–108.
8. Young AA, Li B, Kirton RS, Cowan BR. Generalized spatiotemporal myocardial strain analysis for DENSE and SPAMM imaging. Magn Reson Med 2012;67:1590–1599.
9. Hor KN, Baumann R, Pedrizzetti G, et al. Magnetic resonance derived myocardial strain assessment using feature tracking. J Vis Exp 2011 [Epub ahead of print].
10. Hor KN, Gottliebson WM, Carson C, et al. Comparison of magnetic resonance feature tracking for strain calculation with harmonic phase imaging analysis. JACC Cardiovasc Imaging 2010;3: 144–151.
11. Morton G, Schuster A, Jogiya R, Kutty S, Beerbaum P, Nagel E. Inter-study reproducibility of cardiovascular magnetic resonance myocardial feature tracking. J Cardiovasc Magn Reson 2012;14: 43.
12. Schuster A, Paul M, Bettencourt N, et al. Cardiovascular magnetic resonance myocardial feature tracking for quantitative viability assessment in ischemic cardiomyopathy. Int J Cardiol 2013;166:413–420.
13. Schuster A, Kutty S, Padiyath A, et al. Cardiovascular magnetic resonance myocardial feature tracking detects quantitative wall motion during dobutamine stress. J Cardiovasc Magn Reson 2011;13:58.
14. Harrild DM, Han Y, Geva T, Zhou J, Marcus E, Powell AJ. Comparison of cardiac MRI tissue tracking and myocardial tagging for assessment of regional ventricular strain. Int J Cardiovasc Imaging 2012;28:2009–2018.
15. Augustine D, Lewandowski AJ, Lazdam M, et al. Global and regional left ventricular myocardial deformation measures by magnetic resonance feature tracking in healthy volunteers: comparison with tagging and relevance of gender. J Cardiovasc Magn Reson 2013;15:8.
16. Assomull RG, Prasad SK, Lyne J, et al. Cardiovascular magnetic resonance, fibrosis, and prognosis in dilated cardiomyopathy. J Am Coll Cardiol 2006;48:1977–1985.
17. Maceira AM, Prasad SK, Khan M, Pennell DJ. Normalized left ventricular systolic and diastolic function by steady state free precession cardiovascular magnetic resonance. J Cardiovasc Magn Reson 2006;8:417–426.
18. Young AA, Cowan BR, Thrupp SF, Hedley WJ, Dell'Italia LJ. Left ventricular mass and volume: fast calculation with guide-point modeling on MR images. Radiology 2000;216:597–602.
19. Li B, Young AA, Cowan BR. GPU accelerated non-rigid registration for the evaluation of cardiac function. Med Image Comput Comput Assist Interv 2008;11:880–887.
20. Li B, Liu Y, Occleshaw CJ, Cowan BR, Young AA. In-line automated tracking for ventricular function with magnetic resonance imaging. JACC Cardiovasc Imaging 2010;3:860–866.
21. Kempny A, Fernandez-Jimenez R, Orwat S, et al. Quantification of biventricular myocardial function using cardiac magnetic resonance feature tracking, endocardial border delineation and echocardiographic speckle tracking in patients with repaired tetralogy of Fallot and healthy controls. J Cardiovasc Magn Reson 2012;14:32.
22. Grothues F, Smith GC, Moon JC, et al. Comparison of interstudy reproducibility of cardiovascular magnetic resonance with two-dimensional echocardiography in normal subjects and in patients with heart failure or left ventricular hypertrophy. Am J Cardiol 2002;90:29–34.
23. Kane GC, Karon BL, Mahoney DW, et al. Progression of left ventricular diastolic dysfunction and risk of heart failure. JAMA 2011;306:856–863.
24. Geyer H, Caracciolo G, Abe H, et al. Assessment of myocardial mechanics using speckle tracking echocardiography: fundamentals and clinical applications. J Am Soc Echocardiogr 2010;23: 351–369; quiz 453–455.
25. Edvardsen T, Rosen BD, Pan L, et al. Regional diastolic dysfunction in individuals with left ventricular hypertrophy measured by tagged magnetic resonance imaging—the Multi-Ethnic Study of Atherosclerosis (MESA). Am Heart J 2006;151:109–114.
26. Moore CC, Lugo-Olivieri CH, McVeigh ER, Zerhouni EA. Three-dimensional systolic strain patterns in the normal human left ventricle: characterization with tagged MR imaging. Radiology 2000;214:453–466.
27. Simonetti OP, Raman SV. Straining to justify strain measurement. JACC Cardiovasc Imaging 2010;3:152–154.
28. Maron BJ, Towbin JA, Thiene G, et al. Contemporary definitions and classification of the cardiomyopathies: an American Heart Association Scientific Statement from the Council on Clinical Cardiology, Heart Failure and Transplantation Committee; Quality of Care and Outcomes Research and Functional Genomics and Translational Biology Interdisciplinary Working Groups; and Council on Epidemiology and Prevention. Circulation 2006;113: 1807–1816.